Research on Chemical Intermediates (2022) 48:3039–3060
https://doi.org/10.1007/s11164-022-04732-7

# Anchoring Cu (II) on $Fe_3O_4$@ $SiO_2$/Schiff base: a green, recyclable, and extremely efficient magnetic nanocatalyst for the synthesis of 2-amino-4H-chromene derivatives

**Saeed Yazdanseta**[1] · **Kosar Yasin**[1] · **Moslem Setoodehkhah**[2] · **Mohammad Ghanbari**[1] · **Elham Fadaee**[2]

Received: 10 January 2022 / Accepted: 24 April 2022 / Published online: 18 May 2022
© The Author(s), under exclusive licence to Springer Nature B.V. 2022

## Abstract

In this work, a novel water-soluble Salen type Cu(II) Schiff base complex functionalized silica-coated magnetite nanoparticles [$Fe_3O_4$@$SiO_2$/Schiff base of Cu(II)] was synthesized and characterized. First, an immobilized water-soluble Schiff base was synthesized from the condensation reaction between 3-amino propyl triethoxy silane (APTES) functionalized silica-coated magnetite nanoparticles and a water-soluble aldehyde (sodium salicylaldehyde-5-sulfonate monohydrate). After that, functionalized Schiff base was converted to functionalized Cu(II) Schiff base complex as the result of reaction with Cu(II) acetate tetrahydrate. The structural and magnetic properties of the prepared compounds were identified by FT-IR, XRD, SEM, EDX, TEM, VSM, and TGA. The catalytic activity of the novel nanocatalyst was investigated for the preparation of 2-amino-4H-chromene derivatives through an one-pot, three-component reaction of dimedone, aromatic aldehydes, and malononitrile, in the presence of catalytic amounts of the $Fe_3O_4$@$SiO_2$/Schiff base of Cu(II) nanocatalyst in water and at room temperature. The 2-amino-4H-chromene derivatives were obtained in good to excellent yields. Furthermore, because of the solubility of metal Schiff base complexes in water, the nanocatalyst dispersed in water easily without using ultrasonic or shaker.

**Keywords** Eco-friendly catalyst · 2-amino-4H-chromene · Multi-component reaction · $Fe_3O_4$@$SiO_2$-Schiff-base · $Fe_3O_4$ nanoparticles · Cu(II)

---

✉ Moslem Setoodehkhah
setoodehkhah@kashanu.ac.ir

✉ Mohammad Ghanbari
ghanbari-m@kashanu.ac.ir

[1] Department of Organic Chemistry, Faculty of Chemistry, University of Kashan, Kashan, Iran

[2] Department of Inorganic Chemistry, Faculty of Chemistry, University of Kashan, Kashan, Iran

## Introduction

Heterocyclic compounds with the chromene moiety, widely present in edible fruits and vegetables, have demonstrated interesting characteristics, rendering them attractive targets for chemical synthesis [1]. Among various derivatives of chromene, 2-amino-4H-chromene derivatives have attracted great attention, as they present wide range of biological and pharmacological functions such as antimicrobial [2], antitumor [3], antifungal [4], anticancer [5], antileishmanial [6], antioxidant [7], inhibitors [8], and hypotensive activities [9]. Thus, the introduction of efficient procedures with easily separable, eco-friendly, and reusable catalysts for the synthesis of these derivatives is highly demanded.

Catalyst plays a crucial role in chemical processes, industrial and academic laboratories and various organic transformations. Recently, the applications of homogeneous catalysts in organic reactions have been limited due to difficulties in their reusability and recovery. For these reasons, the heterogeneous versions of catalysts have been developed [10, 11]. However, the activity of heterogeneous catalysts is less than their homogeneous counterparts. The solution to overcome this problem is the use of nanomaterials [12, 13]. Nowadays, the nanomaterials are widely used in sciences such as chemistry, physics, biology, biomedicine, biotechnology environmental areas, and material science [14–20]. In this context, magnetic nanoparticles (MNPs) have been prominent because of their unique properties including superparamagnetism, high magnetic susceptibility, and low curie temperature [21, 22]. Among MNPs, $Fe_3O_4$ nanoparticles are a good candidate as a support material due to their exclusive properties such as the abundance of unique activities, low price and toxicity, simple synthesis and functionalization, large surface area, biocompatibility, and easy separation with a magnetic field [23–27]. However, in order to prevent $Fe_3O_4$ nanoparticles from self-aggregation and oxidation, they are shielded by a suitable coating through surface functionalization. Silica is one of the most promising candidates for surface coating of nanoparticles [28]. The shell of silica protects the inner magnetite core from oxidation and provides the sites for surface functionalization with various functional groups [29].

In recent decades, the Schiff base ligands have been played the prominent roles in organic and inorganic chemistry and in transition metal coordination chemistry [30–32]. The advantages of these ligands are that they make the stable complexes with the most transition metals and have great efficiency as catalysts [33–35]. Schiff base transition metal complexes are also used extensively for industrial purposes and have broad biological applications [36, 37]. Various structures with the desired shell such as metal Schiff base complexes and magnetic core can be prepared and used for catalytic applications. Recently, magnetic nanoparticles functionalized with metal Schiff base complexes have been developed as an efficient and highly recyclable catalyst [38–40]. Synthesis of various materials supported on magnetic nanoparticles and their use as catalysts for the synthesis of 2-amino-4H-chromene derivatives have been the subject of several kinds of literature [41–46]

As part of our ongoing research program on the development of efficient methods for the preparation of biologically active compounds [47–49], in this work, a

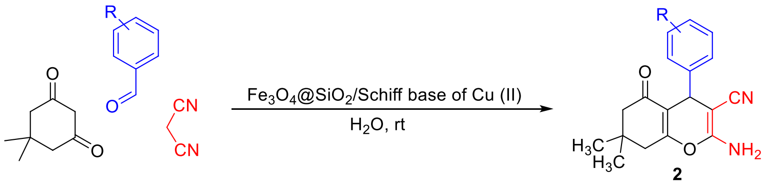

**Scheme 1** General method for preparation 2-amino-4H-chromene derivatives **2**

water-soluble Schiff base complex of Cu(II) functionalized silica-coated magnetite nanoparticles ($Fe_3O_4$@$SiO_2$/Schiff base of Cu(II)) was synthesized and fully characterized. It is noticeable that, because of the solubility of the Schiff base complex in water, this nanocatalyst is dispersed in water easily without using ultrasonic or shaker. This structure was used as an efficient catalyst for green and one-pot synthesis of 2-amino-4H-chromene derivatives. To the best of our knowledge, there are no examples that a water-soluble Schiff base supported on MNPs has been used as a catalyst for the synthesis of 2-amino-4H-chromene derivatives in water at room temperature (Scheme 1).

## Experimental

### Materials and instrumentation

All starting materials, solutions and reagents were purchased from commercial sources (Merck, Sigma Aldrich and fluka) and were used without further purification. Melting points were measured by the Electro thermal 9100 and reported uncorrected. Fourier transform infrared (FT-IR) spectra from 250 to 4000 $cm^{-1}$ were registered using a Perkin-Elmer 781 FT-IR Spectrometer, using KBr pellets. $^1H$ NMR spectra were recorded with a Bruker Avance DPX 400 MHz spectrometer in $CDCl_3$ as solvent in the presence of TMS as the internal standard. X-ray powder diffraction analysis (XRD) measurements were obtained on a STADI P diffractometer (STOE, Germany) using Cu Kα radiation with a scanning rate of 3° $min^{-1}$ in the $2\theta$ range between 10° and 80°. The morphology and size of the nanoparticles were observed on a Zeiss-XL-30 field emission scanning electron microscope (FE SEM). Transmission electron microscopy (TEM) images were obtained on a Zeiss EM10C with an accelerating voltage of 100 kV. Magnetic susceptibility measurements were carried out using a vibrating sample magnetometer (VSM, Meghnatis Daghigh Kavir Company, Iran) in the magnetic field at room temperature. The TGA curves were recorded by a Rheometric Scientific Inc. 1998 thermal analysis apparatus under an $N_2$ atmosphere.

### Preparations of $Fe_3O_4$ nanoparticles (MNPs) and $Fe_3O_4$@$SiO_2$

Magnetite nanoparticles (MNPs) were prepared according to the previous report [25]. Briefly, $FeCl_3.6H_2O$ (2.70 g, 10 mmol) and $FeCl_2.4H_2O$ (1.0 g, 5 mmol) were

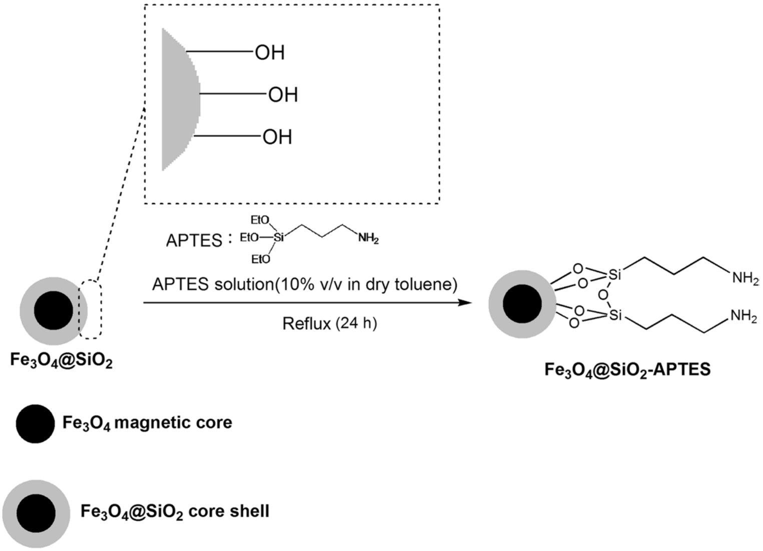

**Scheme 2** A schematic diagram for the synthesis of $Fe_3O_4$@$SiO_2$-APTES

dissolved in 30 mL of deionized water, degassed with nitrogen gas for 15 min. The resultant solution was left to be stirred for 0.5 h at 80 °C. Then 25% ammonia solution was added dropwise until reaction media reached pH 10. After 15 min, the solid was separated by a magnet and washed three times with deionized water and ethanol and then dried under vacuum at 70 °C for 12 h. The product is black.

The $SiO_2$ layer was prepared through a modified Stober method [25]. Briefly, (1.5 g, 6.3 mmol) MNPs were dispersed in a mixture of deionized water (10 mL), and ethanol (50 mL). Then Tetraethoxysilane (TEOS) (0.60 mL) was added and followed by the addition of 15.0 mL of NaOH (10 wt%) under stirring. The mixture was stirred mechanically for 45 min at 35 °C temperature. Afterward, the obtained product was separated by applying an external magnet, washed three times with deionized water and ethanol and dried under vacuum at 60 °C for 24 h. the product is brown at this stage.

## Functionalizing of silica-coated MNPs with APTES ($Fe_3O_4$@$SiO_2$-APTES)

$Fe_3O_4$@$SiO_2$–APTES was prepared according to the previous report [50]. Briefly, 0.5 g of $Fe_3O_4$@$SiO_2$ was suspended in 5 mL (3-aminopropyl)triethoxysilane (APTES) solution (10% v/v in dry toluene) by ultrasonication for 15 min. The mixture was stirred under reflux condition at 110 °C for 24 h. Then it was cooled to room temperature, the sample was separated by applying an external magnet, washed three times with toluene and deionized water to remove unreacted APTES. Finally, the sample was dried under vacuum at 80 °C for 24 h. The schematic diagram for the synthesis of products is shown in Scheme 2.

## Synthesis of sodium salicylaldehyde-5- sulfonate monohydrate (Sals)

Aldehyde used in this work is sodium salicylaldehyde-5-sulfonate monohydrate (Sals) which is a water-soluble aldehyde. This aldehyde was synthesized and characterized according to the modified previous report [51]. Briefly, a mixture of salicylaldehyde (0.9 g, 7.37 mmol) and aniline (0.86 g, 9.21 mmol) in methanol (25 mL) is heated at reflux for 3 h. During this time a yellow precipitate of *N*-Phenylsalicylaldimine is formed. The product is isolated and recrystallized in methanol. At the next step, 1.0 g of *N*-phenylsalicylicaldimine is added to 2.4 mL of concentrated sulfuric acid and heated at 100 °C for 2 h under stirring. After heating, the solution is cooled to room temperature and then is poured into the ice water while continuously stirring. Yellow precipitate (*N*-phenylsalideneimine-5-sulfonic acid) is formed and recrystallized in dilute sulfuric acid. To convert sulfonic acid substitution to sodium sulfonate, the product of the previous step (*N*-phenylsalideneimine-5-sulfonic acid) is dissolved in an aqueous solution of sodium carbonate and boiled in an open flask for 2.5 h. Acetic acid is added slowly to the cooled solution until the pH reached 5. At the last step of this synthesis, ethanol is added and the mixture is cooled to 0 °C. The yellow precipitate, sodium salicylaldehyde-5-sulfonate, was obtained and filtered off. The synthesized aldehyde (Sals) is a water-soluble product. The product was characterized by $^1$H NMR and FT-IR spectrometry.

## Synthesis of $Fe_3O_4$@$SiO_2$/Schiff base

0.5 g of $Fe_3O_4$@$SiO_2$-APTES was suspended in a solution of sodium salicylaldehyde-5-sulfonate monohydrate (Sals) (0.28 g (1 mmol) in 35 mL hot ethanol) by ultrasonication for 15 min. The mixture was stirred under reflux condition at 110 °C for 24 h. After it was cooled to room temperature, the sample was separated by an external magnet and washed three times with 5 mL ethanol and 2.5 mL deionized water to remove unreacted Sals. Finally, the sample was dried under vacuum at 80 °C for 12 h. The product is $Fe_3O_4$@$SiO_2$ nanoparticles functionalized by a water-soluble Schiff base ligand. FT-IR spectrum of the product showed the expected bands, including a distinctive band due to –C=N stretching.

## Synthesis of $Fe_3O_4$@$SiO_2$/Cu Schiff base complexes

1.2 g of $Fe_3O_4$@$SiO_2$/Schiff base was suspended in 60 mL ethanol by ultrasonic for 20 min. Then, 0.6 g of Cu $(CH_3COO)_2 \cdot H_2O$ was added dropwise to it. The mixture was refluxed 24 h. After this time, the product (a dark solid) was removed from the solvent by a strong external magnet, washed with deionized water and ethanol and subsequently dried under vacuum at 80 °C for 12 h. A schematic diagram for the synthesis of $Fe_3O_4$@$SiO_2$/Schiff base of Cu (II) is shown in Scheme 3.

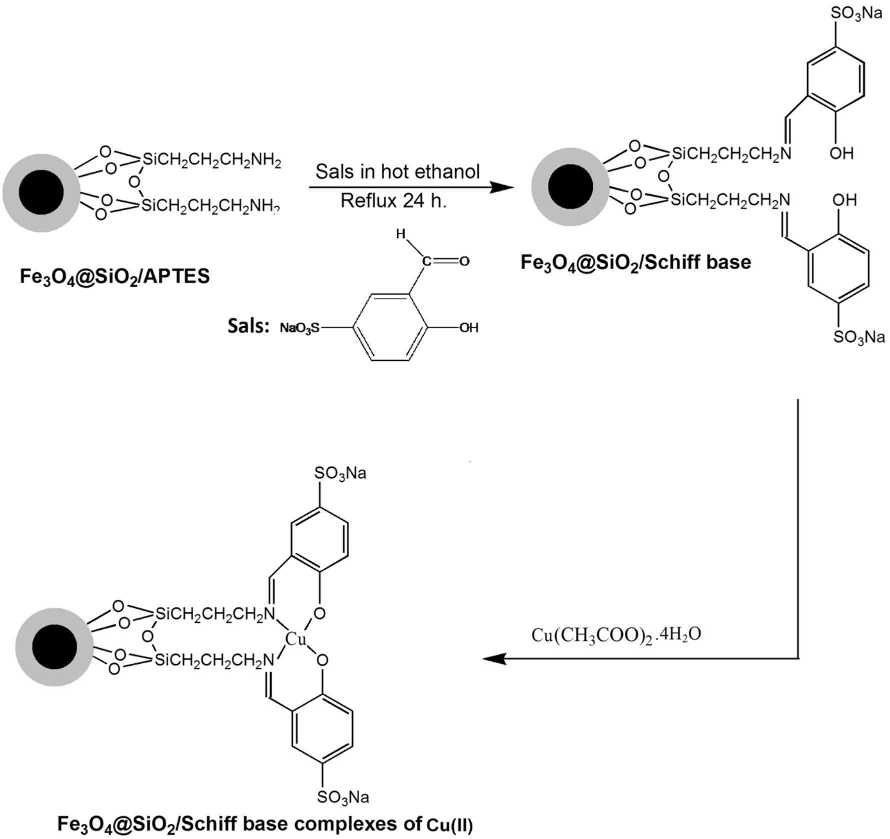
Fe3O4@SiO2/APTES
SiCH2CH2CH2NH2
Sals in hot ethanol
Reflux 24 h.
Sals:
NaO3S
OH
Fe3O4@SiO2/Schiff base
SO3Na
OH
Cu(CH3COO)2.4H2O
Cu
Fe3O4@SiO2/Schiff base complexes of Cu(II)

**Scheme 3** Schematic diagram for the synthesis of $Fe_3O_4$@$SiO_2$/Schiff base of Cu (II)

## General procedure for the synthesis of 2‑amino‑4H‑chromene derivatives by using $Fe_3O_4$@$SiO_2$/Schiff base of Cu (II) nanocatalyst

A stoichiometric mixture of an aromatic aldehyde (1.0 mmol), malononitrile (1.0 mmol), dimedone (1.0 mmol), and 5 mL $H_2O$ in the presence of 10 mg of the $Fe_3O_4$@$SiO_2$/Schiff base of Cu (II) nanocatalyst were mixed thoroughly. The mixture was stirred at room temperature for an appropriate time (Table 3). After completion of the reaction confirmed by TLC, solid catalyst was separated by an external magnet and the solution was filtered and washed with ethanol and dried under vacuum. The precipitate was purified by recrystallization with ethanol, gave the pure products in 87–98% yields based on the starting aromatic aldehyde. The products were characterized by IR, $^1$H NMR and via comparison of their melting points with the previously reported.

## Result and discussions

### Structural characterization of $Fe_3O_4$@$SiO_2$/Schiff base of Cu(II) nanocatalyst

The FT-IR spectra of $Fe_3O_4$, $Fe_3O_4$@$SiO_2$, $Fe_3O_4$@$SiO_2$/APTES, Sals, $Fe_3O_4$@ $SiO_2$/Schiff base and $Fe_3O_4$@$SiO_2$/Schiff base of Cu(II) are shown in Fig. 1. The vibration bands at 579–635 $cm^{-1}$ are assigned to (Fe–O) stretching [52] Fig. 1a, b, c, e, f. The weak vibration band at around 1629 $cm^{-1}$ in the spectra of $Fe_3O_4$ and $Fe_3O_4$@$SiO_2$ is assigned to –OH bending of $H_2O$ molecule. The strong band near 1100 $cm^{-1}$ (Fig. 1b, c, e, f) is assigned to Si–O–Si stretching vibration and demonstrates the formation of silica layer on the surface of MNPs [50]. The presence of a band with medium intensity at around 1624 $cm^{-1}$ in the spectrum of $Fe_3O_4$@ $SiO_2$/APTES is assigned to the bending of the $NH_2$ group of APTES which overlaps with the vibration at 1629 $cm^{-1}$ related to the bending of $H_2O$ molecule and increases its intensity. Furthermore, the vibration bands at 2857 and 2923 $cm^{-1}$ which are assigned to symmetrical and asymmetrical stretching of –$CH_2$-groups respectively, beside the vibration band at 1445 $cm^{-1}$ which is assigned to scissoring vibration of –$CH_2$-groups of APTES, demonstrate –$NH_2$ group functionalized MNPs silica layer. Therefore, these FT-IR spectra (Fig. 1a–c) prove the formation of silica layer on MNPs. The FT-IR spectrum of Sals (Fig. 1d) shows important and specified bands at 1106–1221 $cm^{-1}$ which are caused by symmetrical and asymmetrical stretching of S–O at –$SO_3^-$ substitution and a band at 1661 $cm^{-1}$ which is caused by stretching of C=O group of aldehyde, the band at 3432 $cm^{-1}$ can be assigned to the stretching of –OH in Sals [53]. Successful functionalization of $Fe_3O_4$@$SiO_2$ with water-soluble Schiff base and its complex are proven by the vibration bands at 1033–1037, 1109–1112, and 1166–1175 $cm^{-1}$ related to symmetrical and asymmetrical stretching of S–O at –$SO_3^-$ substitution; In addition, the Schiff base functionalized magnetite silica layer exhibits $\nu$ (C=N) stretch at 1642 $cm^{-1}$ (Fig. 1e). This band shifts to lower frequencies by about 13 $cm^{-1}$ as a result of coordination of the azomethine Schiff base nitrogen atoms to the metal ion[54], The –C=N band at the spectrum of $Fe_3O_4$@$SiO_2$/Schiff base of Cu(II) is seen at 1629 $cm^{-1}$ (Fig. 1f). This shift proves successful coordination of Cu(II) metal ion to functionalized Schiff base ligand. Furthermore, the vibration band which is seen as a shoulder near to Fe–O stretching band at spectrum of metal Schiff base complexes is assigned to Cu–O stretching of Cu(II) Schiff base. The presence of vibration bands at 1456 and 1523 $cm^{-1}$ are assigned to $\nu$ (C=C). Therefore, these FT-IR spectra prove the formation of silica layer on MNPs and also functionalization of magnetite silica layer with water-soluble Schiff base and metal Schiff base complex.

The crystalline structures of the $Fe_3O_4$ nanoparticles and magnetic hybrids were determined by powder X-ray diffraction (XRD). As it can be seen in Fig. 2, all patterns show diffraction peaks at $2\theta = 30.35°$, 35.72°, 43.36°, 53.70°, 57.24°, 62.86°, 71.29° and 73.34°, which correspond to diffractions of (220), (311), (400), (422), (511), (440), (620) and (533) crystallographic faces of magnetite and is consistent with Joint Committee on Powder Diffraction Standards

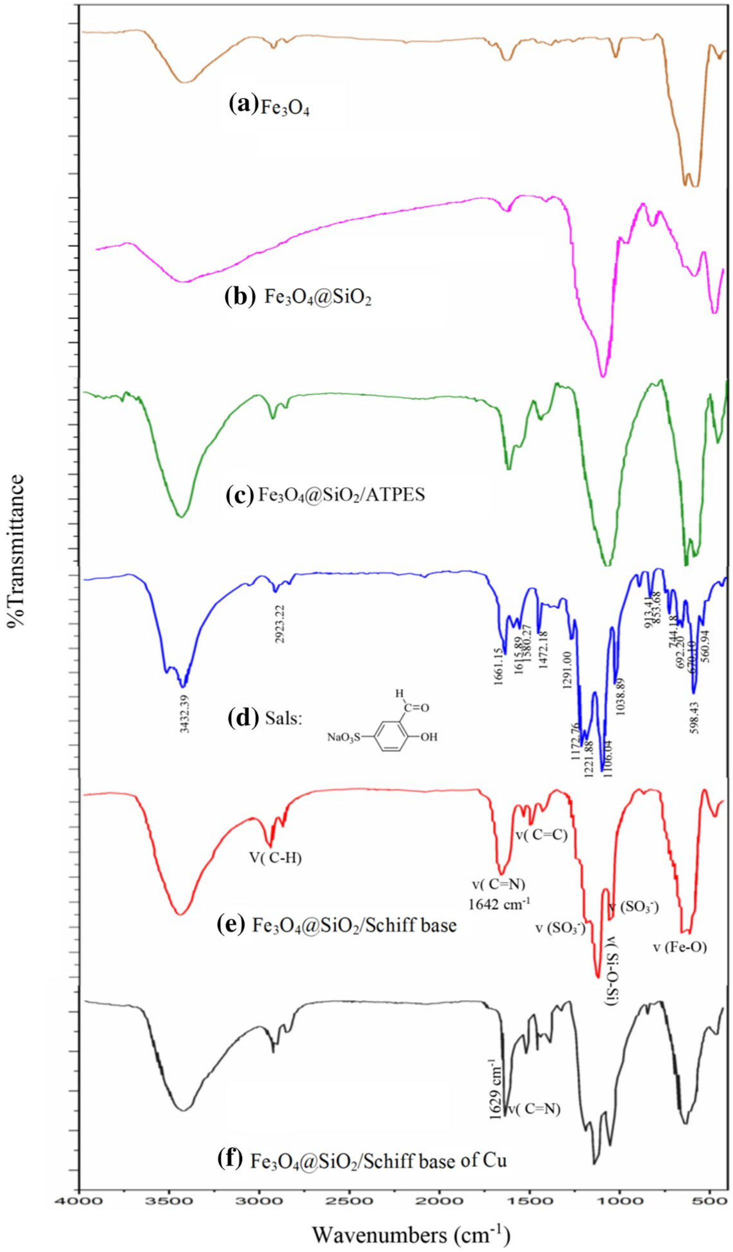

**Fig. 1** FT-IR spectra: **a** $Fe_3O_4$, **b** $Fe_3O_4$@$SiO_2$, **c** $Fe_3O_4$@$SiO_2$ /APTES, and **d** Sals **e** Schiff base ligand functionalized MNPs, and **f** $Fe_3O_4$@$SiO_2$ /Schiff base of Cu(II)

(JCPDS): 750,033. These patterns confirm that the $Fe_3$O4 structure has remained intact after functionalization by Schiff base ligand and metal Schiff base complex on $Fe_3O_4$@$SiO_2$. The average crystallite size of MNPs were also estimated from

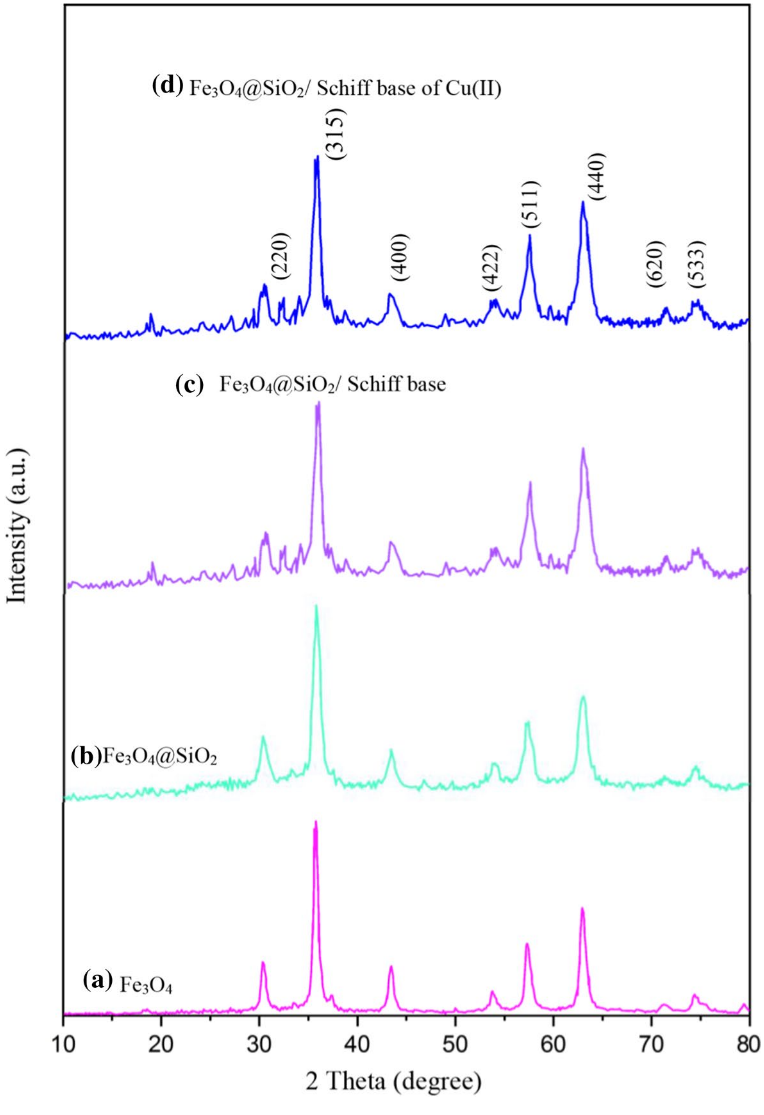

**Fig. 2** XRD patterns: **a** MNPs, **b** $Fe_3O_4$@$SiO_2$, **c** $Fe_3O_4$@$SiO_2$/Schiff base and **d** $Fe_3O_4$@$SiO_2$ Schiff base of Cu(II)

X-ray line broadening using the Scherrer equation ($D=0.9\lambda/\beta\cos\theta$, where $D$ is the average crystalline size, $\lambda$ is the X-ray wavelength used (0.15406 nm), $\beta$ is the angular line width at half maximum intensity, and $\theta$ is the Bragg's angle). For the (311) reflection the average crystalline size of the MNPs was obtained to be around 21 nm.

The size and morphology details of the $Fe_3O_4$@$SiO_2$/Schiff base of Cu(II) were achieved by Field Emission Scanning Electron Microscopy (FE-SEM). As shown

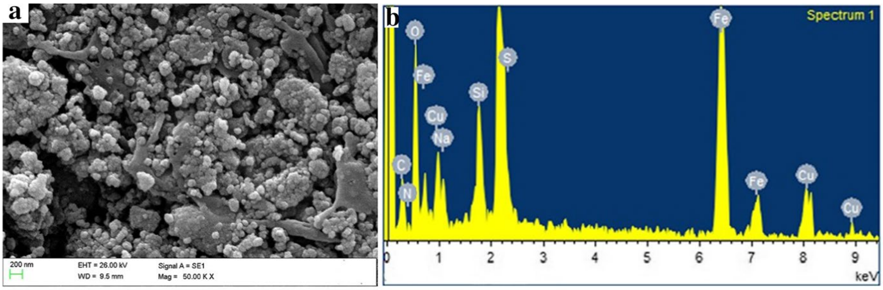

**Fig. 3** SEM image **a** and EDX spectroscopy **b** of $Fe_3O_4$@$SiO_2$/Schiff base of Cu(II)

in Fig. 3, $Fe_3O_4$@$SiO_2$/Schiff base of Cu(II) nanocatalyst don't have uniform shape. This nanocomposite exhibits a mixture of particles with relatively spherical and rod. The size of the sample is approximately in the range of 50–90 nm and the aggregation of particles is seen because of the magnetic properties of the structure. Figure 3 also shows Energy-dispersive X-ray spectroscopy (EDX) of $Fe_3O_4$@$SiO_2$/Schiff base of Cu(II). As shown in Fig. 3, the nanocomposite demonstrates N, C, Na, S atoms related to Schiff Base, besides Fe, Si and O related to $Fe_3O_4$@$SiO_2$. Furthermore, the Cu element has been detected which proves the existence of metal Schiff base complexes on the magnetite silica layer.

Figure 4 displays the TEM image of $Fe_3O_4$@$SiO_2$/Schiff base of Cu (II). As shown in this Fig. the structure of core–shell is obvious here. Additionally, the aggregation of particles is seen because of the magnetic properties of the structure. Due to the aggregation of the particles, it is hard to evaluate the approximate

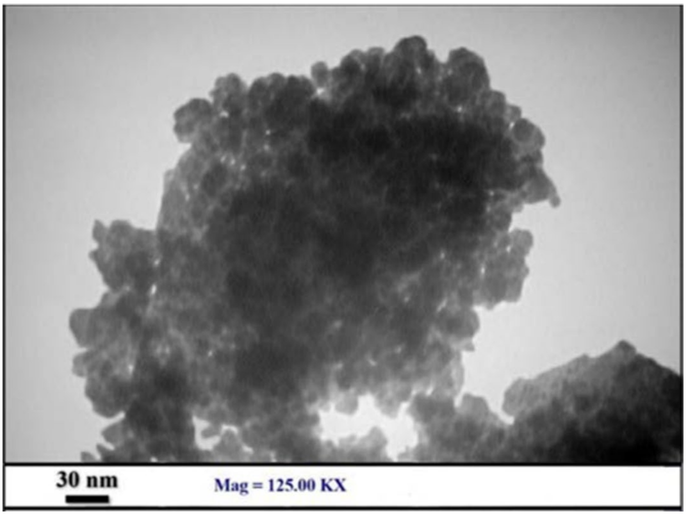

**Fig. 4** TEM image of $Fe_3O_4$@$SiO_2$/Schiff base of Cu(II)

**Fig. 5** VSM curves for the prepared **a** $Fe_3O_4$, **b** $Fe_3O_4$@$SiO_2$/APTES, and **c** $Fe_3O_4$@$SiO_2$/Schiff base of Cu(II)

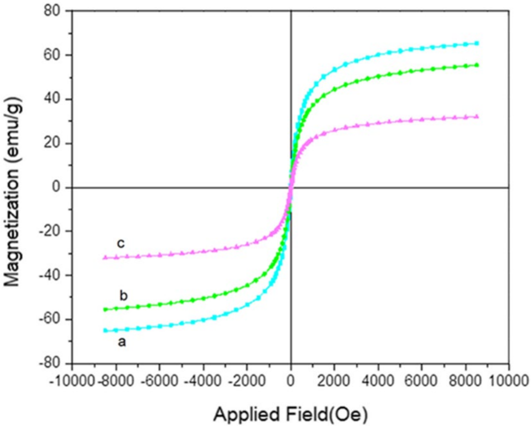

**Fig. 6** TGA curve of $Fe_3O_4$@$SiO_2$/Schiff base of Cu(II)

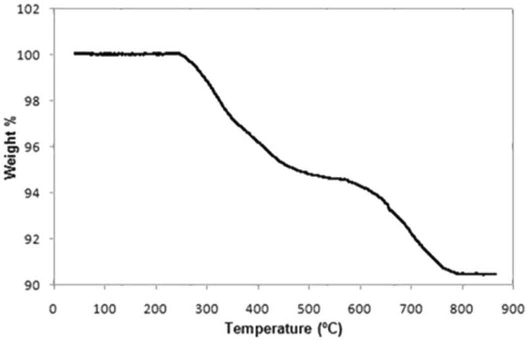

size of all particles, however, several particles, it could be estimated that the nanoparticle size distribution is in the range of 20–30 nm.

The magnetic properties of the nanocomposites that have a magnetic core were demonstrated using a vibrating sample magnetometer (VSM) at 300 K as seen in Fig. 5. The nanocomposites are superparamagnetic at room temperature due to the absence of hysteresis loop in their VSM curves. The magnetic saturation (Ms) values for $Fe_3O_4$, $Fe_3O_4$@$SiO_2$/APTES and $Fe_3O_4$@$SiO_2$/Schiff base of Cu (II) are about 64.87, 54.80 and 31.73 emu/g, respectively. Based on these results the magnetizations are decreased considerably when the coated groups of surface of the $Fe_3O_4$ are increased. Nevertheless, the products have still enough magnetic properties to be separated easily from the solution by an external magnet.

TGA analysis of $Fe_3O_4$@$SiO_2$/Schiff base of Cu (II) was used to estimate the thickness of organic layer coating magnetite silica and the amount of metal Schiff base complex attached onto the surface of $Fe_3O_4$@$SiO_2$ (Fig. 6). As shown in Fig. 6, the weight loss of the nanocomposite up to about 270 ˚C is less than 0.5%, which can be related to the loss of trapped water in the sample or maybe even the small amount of water coordinated to metal center. The weight loss is quite small in this step. The weight loss in the next step is in the range of 270–510 °C.

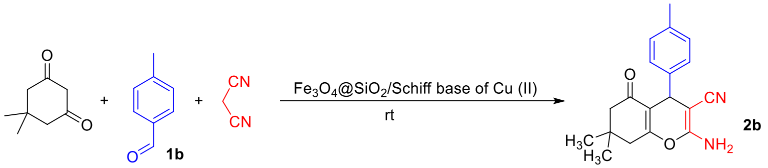

**Scheme 4** Model reaction for the synthesis of 2-amino-4H-chromene **2b**

**Table 1** Effect of different solvents on the synthesis of 2-amino-4H-chromene **2b** in the presence of $Fe_3O_4@SiO_2$/Schiff base of Cu(II) nanocatalyst [a]

| Entry | Solvent | Temperature | Time (min) | Yield (%)[b] |
|---|---|---|---|---|
| 1 | MeCN | r.t | 60 | 65 |
| 2 | EtOH | r.t | 60 | 71 |
| 3 | EtoH-$H_2O$ (1:1) | r.t | 50 | 79 |
| 4 | $H_2O$ | r.t | 50 | 88 |

[a] Reaction conditions: dimedone (1 mmol), 4-methylbenzaldehyde **1b** (1 mmol), malononitrile (1 mmol), solvent (5 mL), r.t

[b] Isolated yield based on **1b**

In this step, the sample loses 5% of its weight and this weight loss can be attributed to the decomposition of some part of the organic layer attached onto the surface of the magnetite silica layer ($Fe_3O_4@SiO_2$). The last step of weight loss is in the range of 600–790 °C. In this step, the nanocomposite loses about 4.5% of its weight. This step, which occurs at high temperatures, can be attributed to the thermal oxidation of carbonaceous residue left on the magnetite silica layer. From the temperature about 780 °C onwards, no weight loss occurs. In this way, the results of TGA show that the total lost weight in this heating process is about 10% of the nanocomposite and it turns out that the Cu(II) Schiff base complex supported on magnetite silica is a thin layer.

## Catalytic activity

In this study, we have synthesized 2-amino-4H-chromene derivatives **2** via one-pot, three-component reaction of dimedone, aromatic aldehydes, and malononitrile, in the presence of catalytic amounts of the $Fe_3O_4@SiO_2$/Schiff base of Cu(II) nanocatalyst in water at room temperature (Scheme 4).

At the outset of our study, to optimize the reaction conditions, a model reaction was carried out by starting from dimedone (1 mmol), 4-methylbenzaldehyde **1b** (1 mmol), and malononitrile (1 mmol) at room temperature (Scheme 2). Various solvents such as acetonitrile, ethanol, mixture of ethanol and water, were investigated for the model reaction in the presence of 10 mg of $Fe_3O_4@SiO_2$/Schiff base of Cu(II) nanocatalyst to find the optimum reaction media (Table 1). It was found that the best result was obtained in the $H_2O$ as a green solvent (Table 1, entry 4).

Next, the catalytic efficiency of the $Fe_3O_4@SiO_2$/Schiff base of Cu(II) nanocatalyst was investigated for the model reaction with different amounts of catalyst (Table 2). To establish the real effectiveness of the catalyst, we studied the

**Table 2** Effect of the catalyst amount for the synthesis of 2-amino-4*H*-chromene **2b** [a]

| Entry | Catalyst | Amount (mg) | Yield (%)[b] |
|---|---|---|---|
| 1 | $Fe_3O_4$@$SiO_2$/Schiff base of Cu(II) | 5 | 62 |
| 2 | $Fe_3O_4$@$SiO_2$/Schiff base of Cu(II) | 10 | 88 |
| 3 | $Fe_3O_4$@$SiO_2$/Schiff base of Cu(II) | 15 | 88 |

[a] Reaction conditions: dimedone (1 mmol), 4-methylbenzaldehyde **1b** (1 mmol), malononitrile (1 mmol), $H_2O$ (5 mL), r.t, 50 min

[b] Isolated yield based on **1b**

model reaction by using 5–15 mg of $Fe_3O_4$@$SiO_2$/Schiff base of Cu(II) nanocatalyst. These results showed that the higher yield was obtained with 10 mg of $Fe_3O_4$@$SiO_2$/Schiff base of Cu(II) as a catalyst (Table 2, entry 2). Therefore, 10 mg of catalyst was found to be the optimal amount and sufficient to produce the best yield of products. As can be seen from Table 2, by increasing and decreasing the amount of nanocatalyst, the yield of the product was not improved (Table 2, entry 1 and 3).

To evaluate the generality of the present protocol for the synthesis of 2-amino-4H-chromene, we investigated the reaction by using a wide range of aromatic aldehydes with various substitutions contains electron-withdrawing, electron-donating, and halogen groups on their aromatic rings under optimized conditions (Table 3). For this aim, aryl benzaldehyde **1** (1.0 mmol) was reacted with dimedone (1 mmol), and malononitrile (1 mmol), in the presence of catalytic amount of the $Fe_3O_4$@$SiO_2$/Schiff base of Cu(II) (10 mg) nanocatalyst in water at room temperature. The structures of all the products were characterized by FT-IR and $^1H$ NMR spectral analysis and their melting points.

## Recyclability of the catalyst

Since catalyst recovery is one of the important goals in organic reactions that reduce waste, and prevents the production of useless and harmful substances for the environment, the recovery and reusability of catalysts must be attended to in catalyst design. For evaluation of recovery catalyst, we use the model reaction, 4-methyl benzaldehyde, malononitrile, and dimedone (molar ratio: 1:1:1). After the completion of the reaction, the catalyst was simply separated from the reaction medium by an external magnet and washed several times with ethanol and acetone. Then it placed in an oven at 70 °C to dry and used in the next reaction. At the end of each reaction, the resulting product was purified and the yield was calculated to compare the catalyst activity each time the reaction was repeated. As can be seen in Fig. 7, the reaction yield did not decrease significantly during five uses of the catalyst. These results showed that the catalyst could be a satisfactory catalyst for this reaction with good reusability and high activity.

**Table 3** Synthesis of 2-amino-4*H*-chromene derivatives **2** via one-pot, three-component reaction in the presence of $Fe_3O_4$@$SiO_2$/Schiff base of Cu(II) nanocatalyst in water [a]

| Entry | Aldehyde | Product | time (min) | Yield (%)[b] | m.p. (obsd.) (°C) | M.p. (lit.) (°C) |
|---|---|---|---|---|---|---|
| 1 | 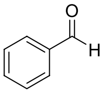 **1a** | 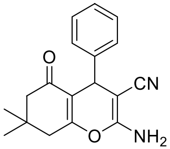 **2a** | 40 | 94 | 227–230 | 219–221 [55] |
| 2 | 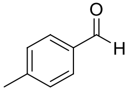 **1b** | 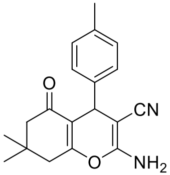 **2b** | 50 | 88 | 220–222 | 211–213 [55] |
| 3 | 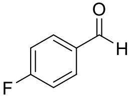 **1c** | 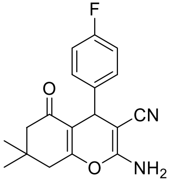 **2c** | 55 | 92 | 185–188 | 188–191 [56] |
| 4 | 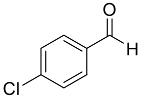 **1d** | 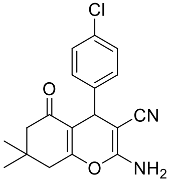 **2d** | 40 | 90 | 212–215 | 206–209 [57] |

**Table 3** (continued)

| Entry | Aldehyde | Product | time (min) | Yield (%)$^b$ | m.p. (obsd.) (°C) | M.p. (lit.) (°C) |
|---|---|---|---|---|---|---|
| 5 | 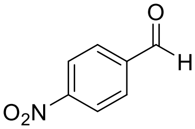 **1e** | 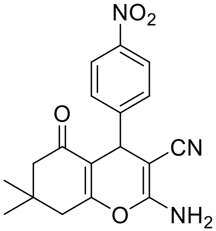 $NO_2$<br>O<br>CN<br>O<br>$NH_2$ **2e** | 35 | 90 | 184–186 | 177–179 [55] |
| 6 | 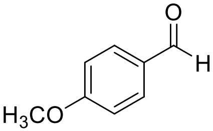 **1f** | 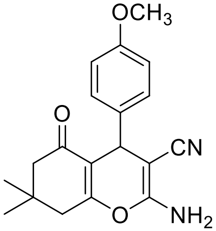 $OCH_3$<br>O<br>CN<br>O<br>$NH_2$ **2f** | 30 | 91 | 203–205 | 197–199[55] |
| 7 | 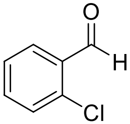 **1g** | 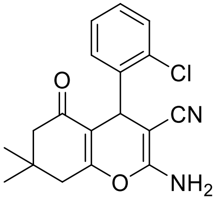 **2g** | 30 | 89 | 209–212 | 204–207 [55] |

**Table 3** (continued)

| Entry | Aldehyde | Product | time (min) | Yield (%)$^b$ | m.p. (obsd.) (°C) | M.p. (lit.) (°C) |
|---|---|---|---|---|---|---|
| 8 | 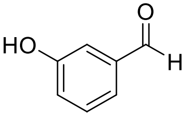 **1h** | 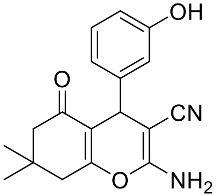 **2h** | 30 | 91 | 230–233 | 225–227 [57] |
| 9 | 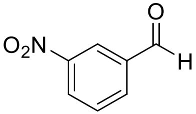 **1i** | 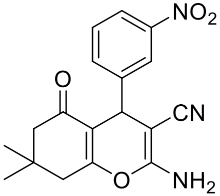 **2i** | 45 | 90 | 206–209 | 206–209[55] |
| 10 | 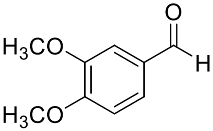 **1j** | 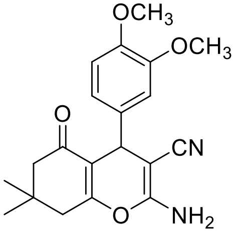 **2j** | 30 | 91 | 170–173 | 169–172 [56] |

**Table 3** (continued)

| Entry | Aldehyde | Product | time (min) | Yield (%)$^b$ | m.p. (obsd.) (°C) | M.p. (lit.) (°C) |
|---|---|---|---|---|---|---|
| 11 | 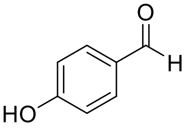 **1k** | 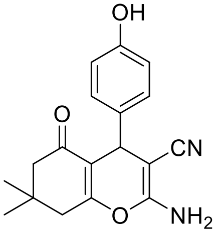 **2k** | 25 | 90 | 200–203 | 205–206 [55] |
| 12 | 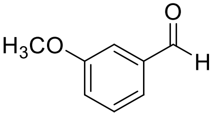 **1l** | 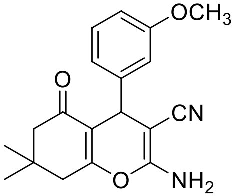 **2l** | 45 | 87 | 203–205 | 197–200 [58] |
| 13 | 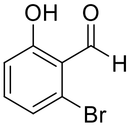 **1m** | 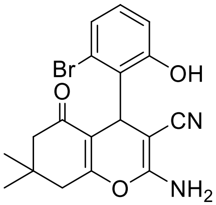 **2m** | 60 | 86 | 213–215 | |

**Table 3** (continued)

| Entry | Aldehyde | Product | time (min) | Yield (%)$^b$ | m.p. (obsd.) (°C) | M.p. (lit.) (°C) |
|---|---|---|---|---|---|---|
| 14 | 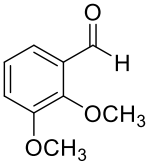 **1n** | 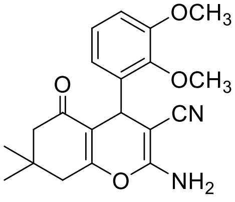 **2n** | 30 | 88 | 211–213 | 212–215 [56] |
| 15 | 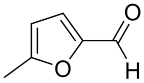 **1o** | 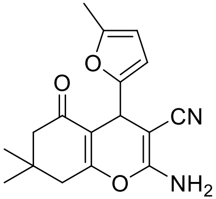 **2o** | 30 | 88 | 203–206 | |
| 16 | 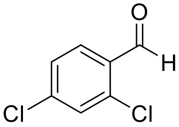 **1p** | 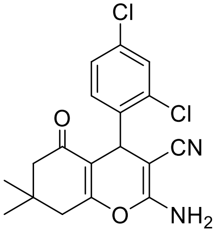 **2p** | 35 | 87 | 165–168 | 163–165 [56] |

[a] Reactions were carried out as described in the experimental section

[b] Isolated yields

**Fig. 7** Reusability of $Fe_3O_4$@$SiO_2$/Schiff base of Cu(II) nanocatalyst in the synthesis of 2-amino-4H-chromene **2b**

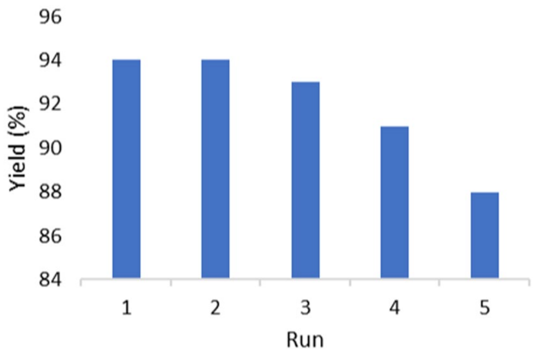

## Comparison of the catalytic efficiency of 2-amino-4H-chromene with other literature reported catalysts

In order to explore the merit of the our method in comparison with other literature methods for the synthesis of the 2-amino-4*H*-chromene compounds, the reaction of 4-methyl benzaldehyde **1b** with malononitrile, and dimedone for the synthesis of the corresponding product were selected as model reaction. The comparison was in terms of solvent, temperature, reaction time, and percentage yields (Table 4). Obviously, the $Fe_3O_4$/$SiO_2$-Schiff base of Cu(II) is a more efficient catalyst with respect to yield, time, solvent and temperature than other literature reported catalysts.

## Proposed reaction pathway for the catalytic system

A plausible mechanism for the synthesis of 2-amino-4*H*-chromene derivatives catalyzed by $Fe_3O_4$/$SiO_2$-Schiff base of Cu (II) is shown in Scheme 5. Initially, malononitrile and aryl aldehyde **1** react with each other via a Knoevenagel condensation reaction. $Fe_3O_4$/$SiO_2$-Schiff base of Cu (II) coordinates with the N and O atoms of malononitrile and aldehyde, respectively, thus increasing the activity of these groups. After passing the dewatering step, it creates alkylidene malononitrile **3**.

**Table 4** Comparison of the catalytic efficiency of $Fe_3O_4$/$SiO_2$-Schiff base of Cu (II) nanocatalyst with reported different catalytic systems for the synthesis of 2-amino-4*H*-chromene **2b**

| Entry | Catalyst | Solvent | Temp | Time (min) | Yield (%) | References |
|---|---|---|---|---|---|---|
| 1 | MMWCNTs-D-$(CH_2)_4$-$SO_3H$ | EtOH | reflux | 15 | 94 | [59] |
| 2 | Horsetail | solvent free | 80 °C | 35 | 86 | [60] |
| 3 | MCM-41@Schiff base-$Co(OAc)_2$ | $H_2O$ | 50 °C | 180 | 94 | [61] |
| 4 | $Fe_3O_4$@$DNH_2$-HPA | EtOH | reflux | 12 | 82 | [62] |
| 5 | POPINO | $H_2O$ | reflux | 20 | 94 | [63] |
| 6 | $NiFe_2O_4$@$SiO_2$–$H_3PW_{12}O_{40}$ | EtOH | reflux | 15 | 89 | [64] |
| 7 | $Fe_3O_4$/$SiO_2$-Schiff base of Cu (II) | $H_2O$ | r.t | 50 | 88 | This work |

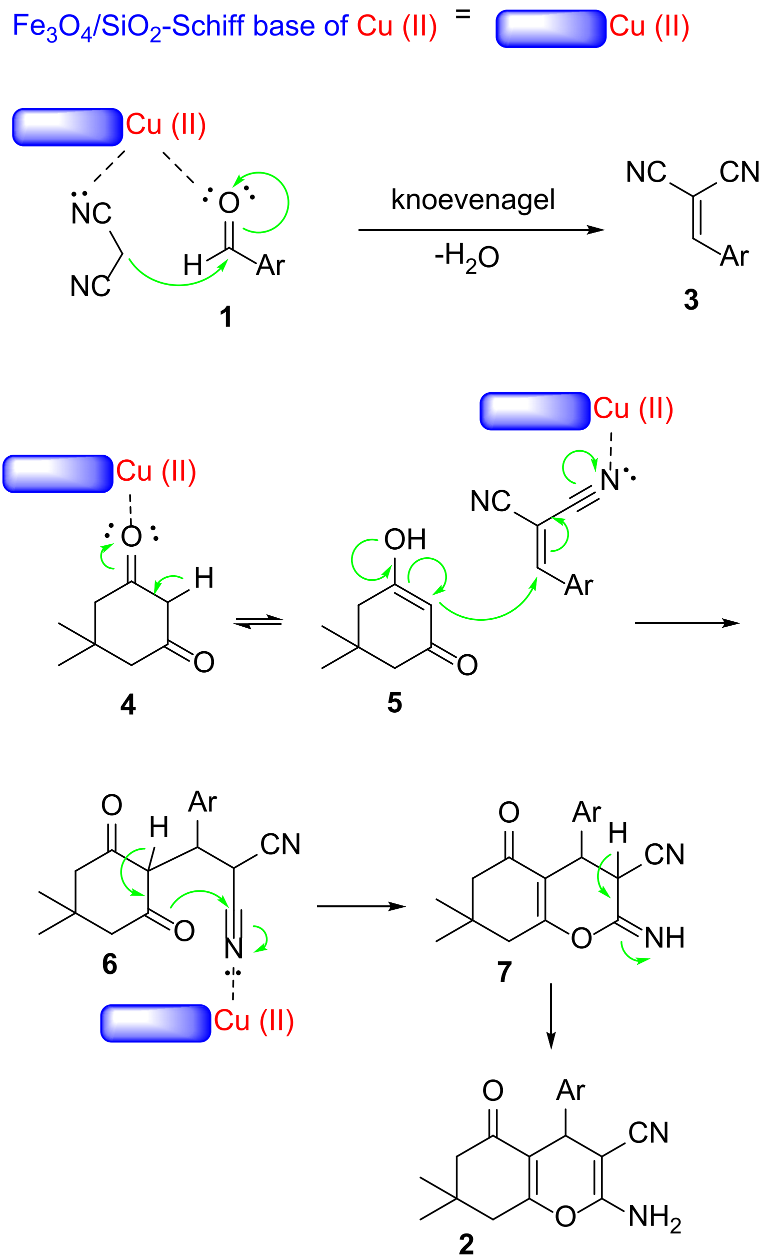
Fe3O4/SiO2-Schiff base of Cu (II) = Cu (II)
Cu (II)
NC
NC
O
H
Ar
1
knoevenagel
-H2O
NC
CN
Ar
3
Cu (II)
O
H
O
4
Cu (II)
N
NC
OH
Ar
O
5
O
H
Ar
CN
O
N
6
Cu (II)
O
Ar
H
CN
O
NH
7
O
Ar
CN
O
NH2
2

**Scheme 5** a plausible mechanism for the synthesis of 2-amino-4H-chromene derivatives 2 in the presence of $Fe_3O_4$@$SiO_2$/Schiff base of Cu(II) as the catalyst

The C-H-activated acid **4** has enol-keto equilibrium with **5**. The Michael addition of intermediate **3** which is activated by $Fe_3O_4/SiO_2$-Schiff base of Cu (II) creates intermediate **6**. This compound is converted to product **2** through a cyclization reaction.

## Conclusions

Cu(II) immobilized on $Fe_3O_4$ nanoparticles coated with Schiff base was prepared as a novel water-soluble, green, inexpensive, and efficient magnetic nanocatalyst. The nanocatalyst was characterized using FT-IR, XRD, SEM, EDX, TEM, VSM, and TGA. The catalytic activity of the catalyst was investigated for the preparation of 2-amino-4H-chromene derivatives through one-pot, three-component reaction of dimedone, aromatic aldehydes, and malononitrile, in the presence of catalytic amounts of the $Fe_3O_4$@$SiO_2$/Schiff base of Cu(II) nanocatalyst in water at room temperature. The 2-amino-4*H*-chromene derivatives were obtained in good to excellent yields and the catalyst was recovered for several runs with little loss in its catalytic performance. Furthermore, because of the solubility of metal Schiff base complexes in water, the nanocatalyst dispersed in water easily without using ultrasonic or shaker. In addition, it can be separated easily with an external magnet from the reaction mixture.

**Supplementary Information** The online version contains supplementary material available at https://doi.org/10.1007/s11164-022-04732-7.

**Acknowledgements** The authors are deeply grateful to the University of Kashan for financial support of this research project.

## Declarations

**Conflict of interest** The authors declare that they have no conflict of interest to disclose.

## References

1. A. Al-Mulla, Der Pharma Chem. **9**, 141 (2017)
2. A. Aminkhani, M. Talati, R. Sharifi, F. Chalabian, F. Katouzian, J. Heterocycl. Chem. **56**, 1812 (2019)
3. Q. Ren, W.Y. Siau, Z. Du, K. Zhang, J. Wang, Chem. Eur. J. **17**, 7781 (2011)
4. S. Agarwal, S. Verma, S.S. Singh, A. Tripathi, Z. Khan, S. Kumar, J. Ethnopharmacol. **71**, 231 (2000)
5. P.K. Paliwal, S.R. Jetti, S. Jain, Med. Chem. Res. **22**, 2984 (2013)
6. T. Narender, S. Gupta, Bioorg. Med. Chem. Lett. **14**, 3913 (2004)
7. T. Symeonidis, M. Chamilos, D.J. Hadjipavlou-Litina, M. Kallitsakis, K.E. Litinas, Bioorg. Med. Chem. Lett. **19**, 1139 (2009)
8. T.H. Huynh, B. Abrahamsen, K.K. Madsen, A. Gonzalez-Franquesa, A.A. Jensen, L. Bunch, Bioorg. Med. Chem. **20**, 6831 (2012)
9. S.X. Cai, J. Drewe, W. Kemnitzer, Anti Cancer Agents Med. Chem. **9**, 437 (2009)
10. M.D. Argyle, C.H. Bartholomew, Catalysts **5**, 145 (2015)
11. M. Nikpassand, M.J. Farshami, J. Cluster Sci. **32**, 975 (2021)
12. N. Sharma, H. Ojha, A. Bharadwaj, D.P. Pathak, P.K. Sharma, RSC Adv. **5**, 53381 (2015)
13. M. Ghanbari, N.M. Dastjerdi, S. Ahmadi, S. Moradi, J. Iran Chem. Soc. **15**, 1119 (2018)
14. N. Mollakarimi-Dastjerdi, M. Ghanbari, Green Chem. Lett. Rev. **13**, 192 (2020)
15. S. Das, B. Sen, N. Debnath, Environ. Sci. Pollut. Res. **22**, 18333 (2015)
16. S.K. Behzad, M.M. Amini, A. Balati, M. Ghanbari, O. Sadeghi, J. Sol-Gel Sci. Technol. **78**, 446 (2016)
17. A.S. Edelstein, R. Cammaratra, *Nanomaterials: synthesis, properties and applications* (CRC Press, 1998)

18. A. Balati, M. Ghanbari, S.K. Behzad, M.M. Amini, Acta Chim. Slov. **64**, 479 (2017)
19. M. Nikpassand, L. Zare-Fekri, L. Karimian, M. Rassa, Curr. Org. Synth. **12**, 358 (2015)
20. Z. Karimi-Jaberi, M.S. Moaddeli, M. Setoodehkhah, M.R. Nazarifar, Res. Chem. Intermed. **42**, 4641 (2016)
21. S.P. Gubin, *Magnetic nanoparticles* (Wiley, 2009)
22. M.-N. Chen, L.-P. Mo, Z.-S. Cui, Z.-H. Zhang, Curr. Opin. Green Sustain. Chem. **15**, 27 (2019)
23. K.N. Koo, A.F. Ismail, M.H.D. Othman, N. Bidin, M.A. Rahman, Malays. J. Fundam. Appl. Sci. **15**, 23 (2019)
24. S.K. Behzad, A. Balati, M.M. Amini, M. Ghanbari, Microchim. Acta **181**, 1781 (2014)
25. M. Ghanbari, S. Moradi, M. Setoodehkhah, Green Chem. Lett. Rev. **11**, 111 (2018)
26. M. Zhang, Y.-H. Liu, Z.-R. Shang, H.-C. Hu, Z.-H. Zhang, Catal. Commun. **88**, 39 (2017)
27. L.Z. Fekri, M. Nikpassand, S.N. Khakshoor, J. Organomet. Chem. **894**, 18 (2019)
28. A. Maleki, Tetrahedron **68**, 7827 (2012)
29. Z. Xi, B. Zheng, C. Wang, Nanosci. Nanotechnol. Lett. **8**, 1061 (2016)
30. X. Liu, J.-R. Hamon, Coord. Chem. Rev. **389**, 94 (2019)
31. Kh. Mohammadi, M. Asadi, M. SetoodehKhah, H. Sepehrpour, Croat. Chem. Acta. **89**, 277 (2016)
32. Z. Asadi, M. Asadi, M. Setoodehkhah, Spectrochim. Acta A Mol. Biomol. Spectrosc. **112**, 214 (2013)
33. M. Asadi, M. SetoodehKhah, J. Iran. Chem. Soc. **7**, 875 (2010)
34. P.G. Cozzi, Chem. Soc. Rev. **33**, 410 (2004)
35. M. Asadi, M. SetoodehKhah, A. Kianfar, J. Iran. Chem. Soc. **7**, 38 (2010)
36. N. Raman, J.D. Raja, A. Sakthivel, J. Chem. Sci. **119**, 303 (2007)
37. M.A. Malik, O.A. Dar, P. Gull, M.Y. Wani, A.A. Hashmi, Med. Chem. Comm. **9**, 409 (2018)
38. J. Rakhtshah, F. Yaghoobi, Int. J. Biol. Macromol. **139**, 904 (2019)
39. S. Rayati, E. Khodaei, M. Jafarian, A. Wojtczak, Polyhedron **133**, 327 (2017)
40. A. Mazraati, M. Setoodehkhah, M. Moradian, J. Inorg. Organomet. Polym. Mater. **32**, 143 (2022)
41. A. Mobinikhaledi, H. Moghanian, Z. Souri, Lett. Org. Chem. **11**, 432 (2014)
42. H. Ebrahimiasl, D. Azarifar, Appl. Organomet. Chem. **34**, 5359 (2020)
43. J. Safari, L. Javadian, Ultrason. Sonochem. **22**, 341 (2015)
44. A. Mobinikhaledi, H. Moghanian, M. Ghanbari, Appl. Organomet. Chem. **32**, 4108 (2018)
45. S. Akocak, B. Şen, N. Lolak, A. Şavk, M. Koca, S. Kuzu, F. Şen, Nano Struct. Nano Objects **11**, 25 (2017)
46. M. Nikpassand, L.Z. Fekri, A. Pourahmad, Lett. Org. Chem. **17**, 360 (2020)
47. M. Ghanbari, E. Kianmehr, S.K. Behzad, S.W. Ng, J. Iran. Chem. Soc. **13**, 7 (2016)
48. S. Ahmadi, M. Ghanbari, Synthesis **53**, 775 (2021)
49. M. Ghanbari, K. Jadidi, M. Mehrdad, N. Assempour, Tetrahedron **72**, 4355 (2016)
50. M. Jafarzadeh, E. Soleimani, P. Norouzi, R. Adnan, H. Sepahvand, J. Fluor. Chem. **178**, 219 (2015)
51. F. Dehghani, A.R. Sardarian, M. Esmaeilpour, J. Organomet. Chem. **743**, 87 (2013)
52. M. Setoodehkhah, S. Momeni, J. Inorg. Organomet. Polym. Mater. **28**, 1098 (2018)
53. N. Monadi, E. Moradi, Transit. Met. Chem. **43**, 161 (2018)
54. M. Tümer, C. Çelik, H. Köksal, S. Serin, Transit. Met. Chem. **24**, 525 (1999)
55. O.H. Qareaghaj, S. Mashkouri, M.R. Naimi-Jamal, G. Kaupp, RSC Adv. **4**, 48191 (2014)
56. N.G. Shabalala, N.P. Hadebe, N. Kerru, S. Maddila, W.E. Van Zyl, S.B. Jonnalagadda, Polycycl. Aromat. Compd. **42**, 505 (2020)
57. R. Hekmatshoar, S. Majedi, K. Bakhtiari, Catal. Commun. **9**, 307 (2008)
58. A. Maleki, Z. Varzi, F. Hassanzadeh-Afruzi, Polyhedron **171**, 193 (2019)
59. F. Adibian, A.R. Pourali, B. Maleki, M. Baghayeri, A. Amiri, Polyhedron **175**, 114 (2020)
60. N.H. Mohtasham, M. Gholizadeh, J. Iran. Chem. Soc. **17**, 397 (2020)
61. S. Pan, P. Li, G. Xu, J. Guo, L. Ke, C. Xie, Z. Zhang, Y. Hui, Res. Chem. Intermed. **46**, 1353 (2020)
62. A. Jamshidi, B. Maleki, F.M. Zonoz, R. Tayebee, Mater. Chem. Phys. **209**, 46 (2018)
63. M.G. Dekamin, M. Eslami, A. Maleki, Tetrahedron **69**, 1074 (2013)
64. B. Maleki, H. Eshghi, M. Barghamadi, N. Nasiri, A. Khojastehnezhad, S.S. Ashrafi, O. Pourshiani, Res. Chem. Intermed. **42**, 3071 (2016)

**Publisher's Note** Springer Nature remains neutral with regard to jurisdictional claims in published maps and institutional affiliations.